From Single to Core-Shell Drops in Non-Confined Microfluidics

Ankur CHAURASIA *, Dimitris JOSEPHIDES, Shahriar SAJJADI

* Corresponding author: Tel.: ++44 (0)7795320616; Email: ankur.chaurasia@kcl.ac.uk
Department of Physics, King's College London, UK

Abstract For many encapsulation applications such as nutrients, cells and drugs, large core-shell drops are required. Conventional confined microfluidic devices are limited to a rather small sized (< 1mm) droplets because of difficulties associated with phase separation at low flow rates. We report a microfluidic device which can produce such large range of drop sizes (~200 μm- 6 mm) with varying shell thickness (~1 μm- 1 mm) under the maximum influence of buoyancy, which has so far remained unexplored. The existing physical model for single drop formation is extended for the core-shell drop. The facile nature of working with such systems means scale up would be easy.

Keywords: Microfluidics, non-confined, Core-shell, Buoyancy

1. Introduction

With the arrival of confined microfluidic techniques for the production of single, double and even higher order emulsions (Utada et al., **2005**; Shah et al., **2008**), the research focus seems to have been shifted away from buoyancy driven drop formation studies (Harkins and Brown **1919**; Scheele and Meister **1968**; Rao et al. **1966**; Walters et al. **1988**; Chazal and Ryan **1971**; Heertjes et al. **1971**; Wang et al. **2009**; Barhate et al. **2004**; Zhang and Stone **1997**; Clanet and Lasheras **1999**) and towards drag dominated approaches that offer good control over scaling down of drop dimensions, high monodispersity and increased drop formation frequency.

All these advantages of confined systems are attractive to several applications demanding small drop size (Shum et al., **2009**; Chen et al., **2012**). However, because of the strong continuous phase flow in the confinement and the problems associated with accumulation of droplets in dead zones due to gravity at low continuous phase flow rates, it is challenging to produce large single and core-shell droplets in these systems which could serve different types of encapsulation applications (Uludag et al., **2000**; Lewinska et al., **2008**; Bremond et al., **2010**).

There have been several works for producing double emulsion droplets using a coaxial capillary set-up (Chang et al. **2009**; Saeki et al. **2010**; Berkland et al. **2004**; Shao et al. **2013**). However, in all these reports, the drag force due to the outer phase flow still limited the drop size to some extent.

We introduce a non-confined microfluidic device that produces giant single and core-shell drops (~200 μm- 6 mm) by taking advantage of the buoyancy and minimizing drag. We also demonstrate a good control over shell thickness *t*, where it was found to vary between ~1 μm – 1 mm. The simple system design having a quiescent outer phase and non-confined geometry would make scale-up easy.

2. Experimental

Materials: Octane (98%, Sigma-Aldrich) was used as the dispersed phase for the single drop experiment and as the middle phase for the core-shell drops. Sodium dodecyl sulphate (SDS; 98.5%, Sigma-Aldrich) was added to the outer water phase for both single and core-shell drop formation. Span85 (Sigma-Aldrich)

was used as surfactant in the middle phase while de-ionised water was used as the inner phase for core-shell drop formation study.

Device: For the single drop experiments, the dispersed oil phase was pumped through a J-type needle (ID: 230 µm, OD: 460 µm) immersed in a vessel containing the continuous water phase. For producing core-shell drops the device used is shown in **Fig. 1**. The tips of inner and middle glass capillaries are axially aligned and placed at the same level. The device is oriented vertically to take advantage of buoyancy and facilitate easy collection of drops.

Both tips were cut and polished to desired lengths. The outer channel had inner and outer tip diameter of 290 µm and 335 µm, respectively, while the inner channel had inner and outer tip diameter of 46 µm and 70 µm, respectively. The axial alignment offset between the two tips was kept within ± 5.0 µm, which left plenty of clearance for the inner phase to remain axisymmetrically engulfed by the middle phase. The outer channel's inner and outer surfaces were selectively treated.

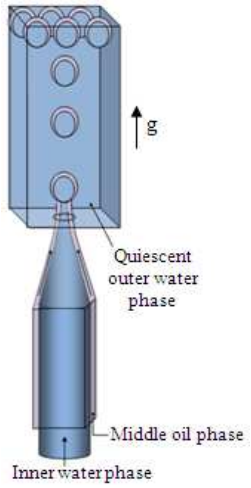

Fig. 1. a) Device schematic for the formation of core-shell drops in a non-confined microfluidic device under the influence of buoyancy.

A circular glass capillary was pulled using a pipette puller (P-1000, Sutter Instrument, Novato USA) and introduced inside a pulled square glass capillary. The inner cross-sectional side length of the square channel was closely equal to the outer diameter of the cylindrical channel which helped in the concentric alignment of their central axes. The coupled and aligned channel set was then introduced inside an open cuvette, which acted as the container for quiescent outer water phase. Device was kept vertical with the tip facing upward, as shown in **Fig. 1**. Drops were collected at the top of cuvette. The drop formation was recorded using a high-speed video camera (Photron Ultima APX Monochrome) while their sizes were measured manually at a downstream position where the drop had stopped wobbling after detaching from the tip and had attained a spherical shape. The coefficient of variation ($\% C_v = 100 \frac{\sigma'}{\mu'}$) was calculated as a measure of the degree of polydispersity where, σ' is the standard deviation of the drop sizes while μ' is their mean.

3. Theory

It is well known that a single drop forming at a tip under the effect of gravity (**Fig. 2a**) experiences buoyancy and kinetic forces acting as disruptive forces, while the interfacial tension holds the drop at the nozzle tip (Harkins and Brown **1919**; Scheele and Meister **1968**). The drag effect in this case is negligible given the quiescent outer continuous phase.

The existing physical model is applied here to a core-shell drop forming under the buoyancy effect in the *dripping* regime (**Fig. 2b**), where it experiences two disruptive kinetic forces (F_{ki} and F_{km}) from the inner and the middle phase flows which can be expressed as,

$$F_{ki} = \rho_i Q_i u_i \;\; ; \;\; F_{km} = \rho_m Q_m u_m \qquad (1)$$

Here ρ is density, Q is volumetric flow rate and u is phase velocity at the tip cross section. The subscripts *i, m* and *o* stand for *inner, middle* and *outer* phase, respectively, throughout the report.

Due to the presence of two interfaces, inner-middle and middle-outer interface (**Fig. 2b**), the cohesive force holding the drop at the tip is increased. The total interfacial force can be expressed as,

$$F_\sigma = \pi d_{w\_i}\sigma(i-m) + \pi d_{w\_o}\sigma(m-o) \quad (2)$$

Here d_{w_i} and d_{w_o} are wetting diameters of inner and outer square channel, respectively, and $\sigma_{(i\text{-}m)}$ and $\sigma_{(i\text{-}m)}$ are the inner/middle interfacial tension and middle/outer interfacial tension, respectively.

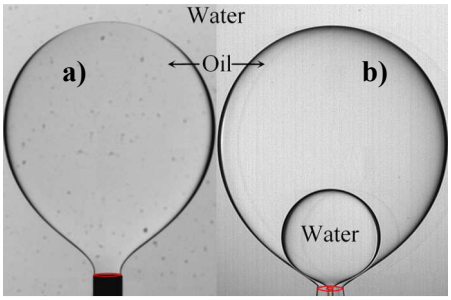

Fig. 2. Formation of a) single and b) core-shell drops in a non-confined microfluidic device under the influence of buoyancy. The red markings indicate the single interfacial tension the holding the single drop in contrast with the presence of two interfaces for the core-shell drop.

Note that here only the oil shell volume contributes to the buoyancy force unlike the single drop where the whole drop volume offered the buoyancy force on the drop to detach. Thus the buoyancy force experienced by the drop is,

$$F_b = \Delta\rho g V_{shell} \quad (3)$$

The term $\Delta\rho$ is the density difference between middle and outer phase. V_{shell} is the shell volume. The total disruptive and the total cohesive forces can be equated to find the drop volume, assuming that the drop detaches once the equality is reached. The shell volume obtained by equating the forces and rearranging the terms is shown below.

$$V_{shell} = \frac{F_\sigma - (F_{ki} - F_{km})}{\Delta\rho g} \quad (4)$$

Assuming the core and the overall drop detach at the same time (also confirmed from the high-speed video recordings), the core volume corresponding to the obtained shell volume can be written as,

$$V_{core} = \frac{Q_i}{Q_m} V_{shell} \quad (5)$$

Using the core and shell volume expressions, the overall drop and core radius can be expressed as,

$$R = \sqrt[3]{\frac{3(V_{shell} + V_{core})}{4\pi}} \quad (6)$$

$$r = \sqrt[3]{\frac{3V_{core}}{4\pi}} \quad (7)$$

4. Results and Discussion

The drop size data for single drops for different oils were explored in different surfactant concentrations in the continuous phase. The drop size predictions obtained by equating the kinetic and buoyancy forces to the interfacial force fit the data well for all the different cases. A typical comparison of the model prediction against the data is shown in **Fig. 4a** for Octane-in-Water system in the absence of surfactants. A good fit of the predicted size for other oils at different interfacial tensions was also noted (Chaurasia et al. **2014a**).

For core-shell drops, different scenarios of surfactant concentrations in middle and outer phases were explored. For a case with very small amount of surfactant in both middle and outer phase (0.1 wt %), it was observed that both the drop and the core size reduced with Q_m at constant Q_i (**Fig. 3b**), which was also observed for a surfactant-free system (**Fig. 4b-c**). In both the scenarios, the drops formed were highly monodisperse, with % C_v < 3%. The drop and core size reduces with Q_m because the critical shell volume needed to detach the drop is reached quicker for high Q_m, thus giving the shell and core less time to develop, thereby reducing the size.

Similarly, the drop and the core size was observed to increase with Q_i at a constant Q_m for the surfactant-free system (**Fig. 4b-c**). In the presence of a small amount surfactant of 0.1 wt% in both, middle and outer, phases (**Fig. 3a**), the rise was observed until the end where the kinetic force reduced the drop and its core size.

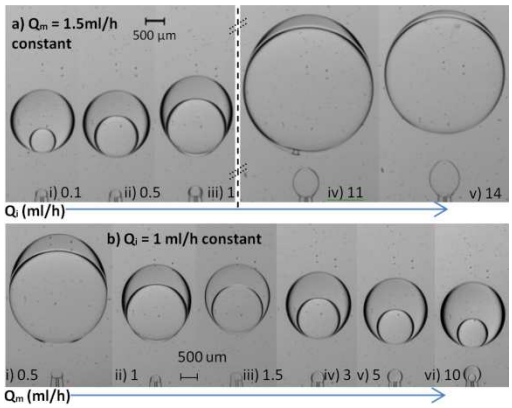

Fig. 3. a) Variation in drop and core sizes shown for increasing Q_i: i) 0.1ml/h, ii) 0.5ml/h, iii) 1ml/h, iv) 11ml/h and v) 14ml/h at fixed Q_m = 1.5ml/h. The dashed line in the middle represents the condition where multi-core polydispersed drops were obtained. b) Reduction in drop and core sizes with increasing Q_m: i) 0.5ml/h, ii) 1ml/h, iii) 1.5ml/h, iv) 3ml/h, v) 5ml/h and vi) 10ml/h at constant Q_i =1ml/h in Region I. The surfactant concentration in both middle and outer phase was 0.1 wt%. Scale bars: 500µm.

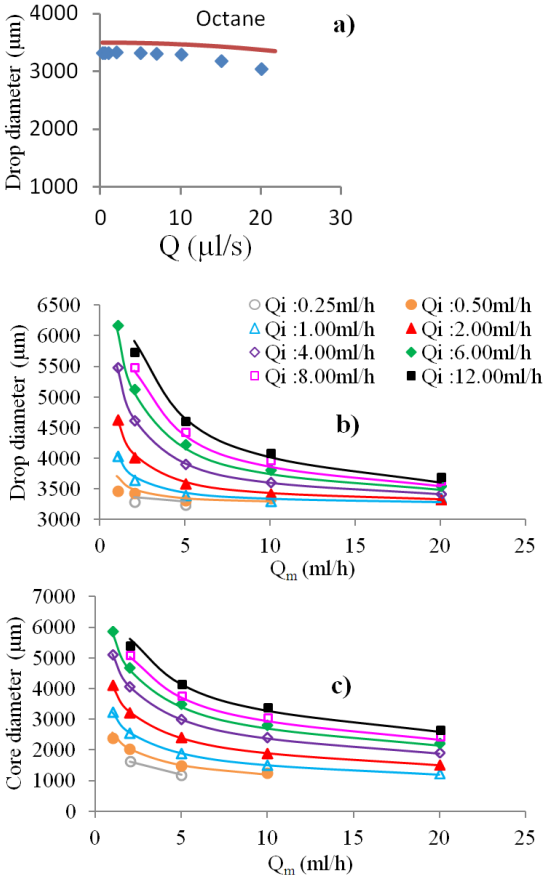

Fig. 4. a) Single drop size data (symbols) for Octane are shown for surfactant-free system (Q: dispersed phase flow rate). b) Drop and c) Core size data (symbols) for the core-shell drops in the surfactant-free system for different oil flow rates. The solid lines show model predictions. The legends for (b) and (c) are common.

At a fixed Q_m, the drop and core size increases with Q_i due to the increase in core size for a given critical shell volume.

To verify and validate the force balance model discussed in the previous section, the drop and core size predictions were compared with the data obtained for the surfactant-free system which avoids the complexities involved in the drop formation in the presence of surfactant. The predictions for the drop and the core size data matched with the experimental data very well as shown in (**Fig. 4b-c**, solid lines). The standard dimensionless numbers, Weber number (*We* = Total kinetic force/Total interfacial tension force) and Bond number (*Bo* = Buoyancy force/Total interfacial tension force), were calculated for the data shown in **Fig. 4**, for which $Bo > 0.85$ and $We < 0.15$ under all the conditions explored. This shows that buoyancy force always remained the dominant force for drop detachment.

Thin shells were obtained in the presence of a small amount of surfactant compared to those obtained in the surfactant-free system. However, these shell thicknesses were still in the order of tens of micrometers. Therefore, in order to achieve even thinner shells, the surfactant concentration was increased further to three different values relative to critical micellar concentration (CMC) in both the oil and the water phase. They are; below CMC (0.4 wt % and 0.2 wt %), at CMC (0.8 wt % and 0.25 wt %), and above CMC (0.8 wt % and 0.5 wt %) for the middle and outer phase, respectively.

Two distinct modes of core-shell drop formation, *dripping* and *jetting*, were observed. The dripping mode was observed only in the below CMC case (**Fig. 5a**) while the jetting mode was observed for all three scenarios. **Fig. 5b** shows drops formed in jetting mode at CMC. The reason why dripping was not observed at CMC and above could be due to a decrease in interfacial tension which facilitates an easier jetting.

It can be seen that low flow rates of the oil

phase were used (introduced via stepper motor controlled syringe pumps) in order to produce ultra-thin shelled drops. As a clarification, no significant fluctuations in the low middle phase flow rates were observed, which was also reflected in the fact that highly monodisperse drops (% C_v < 3%) were produced in *dripping* and *jetting* modes.

The transition from dripping to jetting regime for the below CMC case occurred by increasing the inner phase flow rate. During the jetting mode, the inner phase jets due to its high kinetic force and pulls the middle phase with it, thus creating a biphasic jet. The instability on the jet causes the eventual detachment of the drop at a certain distance from (above) the tip.

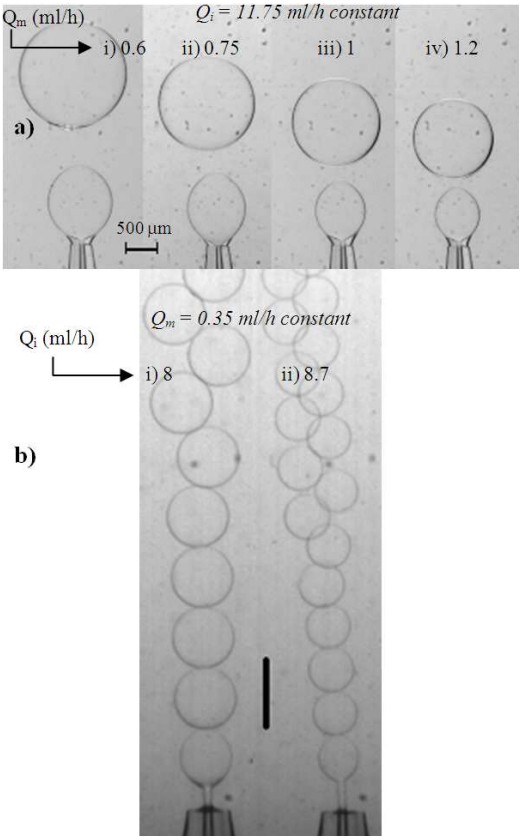

Fig. 5. a) Core-shell drops with ultra-thin shells formed in dripping mode. The drop size decreased with middle phase (oil) flow rate: i) 0.6ml/h, ii) 0.75ml/h, iii) 1ml/h and iv) 1.2ml/h at constant Q_i =11.75ml/h for below CMC case. b) Core-shell drops with ultra-thin shells formed in jetting mode. The drop size decreased with inner phase (water) flow rate: i) 8ml/h and ii) 8.7ml/h for Q_m = 0.35 ml/h at CMC.

Although both regimes produce highly monodisperse droplets, the drops formed in the dripping regime were more monodisperse than the ones formed in the jetting regime.

The drop sizes were controlled with the inner and middle phase flow rates. An increase in the middle phase flow rate increased the drag force on the inner drop and buoyancy force acting on the whole drop and resulted in formation of smaller droplets, as shown in **Fig. 5a**. Similarly, the drop sizes decreased with increasing inner phase flow rate due to a high kinetic force, as shown in **Fig. 5b**.

Due to very thin shells produced in all three scenarios (below, at, and above CMC), their direct measurement was not possible. The times of drop formation (t_f) data, extracted from the high-speed video recordings, were used together with the corresponding Q_i to calculate the core size.

To present the broader context, the variations in shell thickness t with Q_i/Q_m for a wide range of surfactant concentrations are shown in **Fig. 6**, which also includes data for the surfactant-free system and the case with a very small amount of surfactant (0.1 wt% in middle and outer phases).

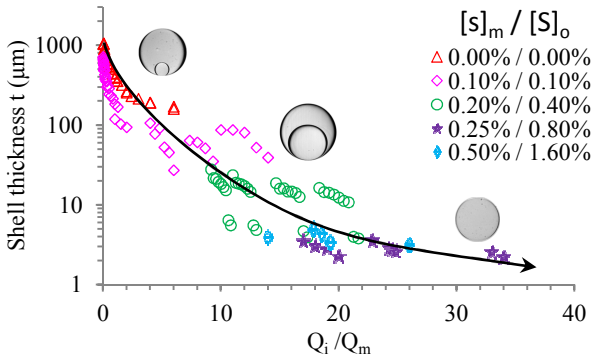

Fig. 6. The range of obtained shell thickness t with inner-to-middle phase flow rate ratio (Q_i/Q_m) is shown for different surfactant concentration cases. $[s]_m$ and $[s]_o$ represent the surfactant concentrations in middle and outer phases respectively.

As a general statement, core-shell drops with rather thick shells (~1 mm) were formed at very low Q_i/Q_m, which was the feasible regime for the surfactant-free and low surfactant concentration case. Highly monodisperse core-shell drops with ultra-thin shells were obtained

up to a maximum core-to-shell volume ratio (Q_i/Q_m) ~35 with the thinnest shell (t~1 μm). Interestingly, this ratio was obtained at CMC. It was observed that the shell thickness below ~1 μm was achievable above CMC at the cost of uniformity. Thus, an optimum interfacial tension condition for obtaining ultra-thin shells is identified, beyond which further reduction in shell thickness is compensated by increase in polydispersity of the drops. A detailed report on the formation of core-shell drops having ultra-thin shells including the trade-off between the shell thickness reduction and the variation in polydispersity has been given elsewhere (Chaurasia and Sajjadi **2014b**).

5. Conclusion

A non-confined microfluidic approach for producing macro core-shell drops with only inner and middle phase flows was introduced. The force-balance model developed for prediction of single drop sizes was extended to predict the drop and core sizes. The model was validated against a surfactant-free system, which avoided the dynamics of interfacial tension, and then was successfully applied to the conditions when surfactants were present. Ultra-thin shelled drops were obtained when the inner phase flow rate became at least approximately ten times the middle phase flow rate. An optimum interfacial tension condition for obtaining drops with thinnest shell (t~1 μm) was identified.

6. References

Barhate RS, Patil G, Srinivas ND and Raghavarao KSMS (2004) Drop formation in aqueous two-phase systems. *Journal of Chromatography A* 1023:197-206

Berkland C, Pollauf E, Pack DW, Kim K, Uniform double-walled polymer microspheres of controllable shell thickness, Journal of controlled release 96 (2004) 101-111

Bremond N., Carreras E.S., Chu L.Y. and Bibette J., Formation of liquid-core capsules having a thin hydrogel membrane: Liquid pearls, *Soft Matter*, 2010, 6, 2484-2488.

Chang Z, Serra C, Bouquey M, Prat L and Hadziioannou G, Co-axial capillaries microfluidic device for synthesizing size- and morphology-controlled polymer core-polymer shell particles, Lab chip, 2009, 9, 3007-3011

Chaurasia A, Josephides D, Sajjadi S, Buoyancy Driven Drop Generation via Microchannel Revisited, 2014a, *submitted*.

Chaurasia A and Sajjadi S, Large Ultra-Thin Shelled Drops via Non-Confined Microfluidics, 2014b, *in preparation.*

Chazal L de, Ryan J (1971) Formation of organic drops in water. *A1ChE J.* 17:1226-1229

Chen P.W., Erb R.M. and Studart A.R., Designer Polymer-Based Microcapsules Made Using Mircofluidics, *Langmuir*, 2012, 28, 144-152.

Clanet C, Lasheras J (1999) Transition from dripping to jetting. *J Fluid Mech* 383:307-326

Harkins W D, Brown FE (1919) The determination of surface tension (free surface energy), and the weight of falling drops- The surface tension of water and benzene by the capillary height method. *Journal of the American Chemical Society* 41:499

Hayworth CB, Treybal RE (1950) Drop Formation in Two-Liquid-Phase Systems. *Industrial & Engineering Chemistry* 42:1174

Heertjes P, Nie L de, Vries H de (1971) Drop formation in liquid-liquid systems - prediction of drop volumes at moderate speed of formation. *Chem Eng Sci* 26:441-449

Lewinska D., Bukowski J., Kozuchowski M., Sinacheiwicz A. and Werinski A., Electrostatic Microencapsulation of Living Cells, *Biocybernetics and Biomedical Engineering*, 2008, 28, 2, 69-84.

Rao EVLN, Kumar R, Kuloor NR (1966) Drop formation studies in liquid-liquid systems. *Chemical Engineering Science* 21:867-880

Saeki D, Sugiura S, Kanamori T, Sato S and Ichikawa S, Microfluidic preparation of water-in-oil-in-water emulsions with an ultra-thin oil phase layer, Lab Chip, 2010, 10, 357–362

Scheele GF and Meister BJ (1968) Drop formation at low velocities in liquid-liquid systems: Part I. Prediction of drop volume. *AIChE J.* 14:9–15

Shah R.K., Shum H.C., Rowat A.C., Lee D., Agresti J.J., Utada A.S., Chu L.Y., Kim J-W., Nieves A.F., Martinez C.J., Weitz D.A., Designer emulsions using microfluidics, *Materials Today*, 2008, vol 11, issue 4, 18-27.

Shao T, Feng X, Jin Y and Cheng Y, Controlled production of double emulsions in dual-coaxial capillaries device for millimetre-scale hollow polymer spheres, Chemical Engineering Science, 2013, 104, 55-63.

Shum H.C., Bandyopadhyay A., Bose S. and Weitz D.A., Double Emulsion Droplets as Microreactors for Synthesis of Mesoporous Hydroxyapatite, *Chem. Mater.* 2009, 21, 5548-5555.

Uludag H., Vos P.D. and Tresco P.A., Technology of mammalian cell encapsulation, *Advanced Drug delivery Reviews* 2000, 42, 29-64.

Utada A.S., Lorenceau E., Link D.R., Kaplan P.D., Stone H.A., Weitz D.A., Monodisperse Double Emulsions generated from a Microcapillary device, *Science,* 308, 537 (2005)

Wang W, Ngan KH, Gong J, Angeli P (2009) Observations on single drop formation from a capillary tube at low flow rates. *Colloids and Surfaces A* 334,1–3:197–202

Zhang DF, Stone HA (1997) Drop formation in viscous flows at a vertical capillary tube. *Phys Fluids* 9:2234